Li_2NiSe_2: A new-type intrinsic two-dimensional ferromagnetic semiconductor above 200 K

Li-Man Xiao(肖丽蔓), Huan-Cheng Yang(杨焕成)[†], and Zhong-Yi Lu(卢仲毅)[‡]

Department of Physics and Beijing Key Laboratory of Opto-electronic Functional Materials Micro-nano Devices, Renmin University of China, Beijing 100872, *China*

(Received 17 September 2022; revised manuscript received 4 November 2022; accepted manuscript online 17 November 2022)

By using first-principles electronic structure calculations, we propose a two-dimensional ferromagnetic semiconductor Li_2NiSe_2 with a Curie temperature above 200 K. The structure of monolayer Li_2NiSe_2 is dynamically stable, which is derived from the synthesized prototype compound Li_2NiO_2 and can be denoted as Li-decorated 1T-type $NiSe_2$. The Ni–Se–Ni ferromagnetic superexchange dominates the magnetic couplings between the Ni atoms, which can be understood in the frame of the Goodenough–Kanamori–Anderson (GKA) rules. Our systematic study of monolayer Li_2NiSe_2 enables its promising applications in spintronics and suggests a new choice to design two-dimensional ferromagnetic semiconductors.

Keywords: two-dimensional ferromagnetic semiconductor, ferromagnetic superexchange, first-principles calculations

PACS: 75.50.Pp, 75.70.Ak, 71.20.–b **DOI:** 10.1088/1674-1056/aca39f

1. Introduction

Ferromagnetic semiconductor materials have attracted a worldwide interest due to their great spin-related application prospects, such as in faster information operation and lower energy consuming devices, spin valves, and magnetic sensors.[1–10] When they are reduced down to atomic-layer thicknesses, namely, two-dimensional ferromagnetic semiconductors (2DFMSs), their sensitive susceptibility to a large variety of external stimuli and their easy integration make them more promising than their bulk counterparts. However, due to the incompatibility between ferromagnetism and semiconductivity, intrinsic 2DFMSs are rare in nature and their Curie temperatures (T_c) are usually much lower than the room temperature, severely hindering their practical applications.[3] So far, only few 2DFMSs have been identified experimentally, such as CrI_3 (45 K),[11] $CrBr_3$ (34 K),[12] $CrCl_3$ (17 K),[13] and $Cr_2Ge_2Te_6$ (bilayer 30 K).[14]

The discovery of 2DFMSs is extremely encouraging, even though there are only few 2DFMSs synthesized and their T_cs are indeed low. Clearly, a critical next step is to find such 2DFMSs which are chemically stable, *i.e.*, can be experimentally synthesized and possess higher T_c. Based on first-principles electronic structure calculations, many kinds of two-dimensional magnetic materials, in different structural prototypes, have been predicted including MAT_3,[15–19] MX_3,[20] and MX_2/MT_2,[21–27] where M refers to transition metals (V, Cr, Mn, Fe, Co, and Ni), A refers to tetrels (Si, Ge, and Sn), T refers to chalcogens (S, Se, and Te), and X refers to halogens (Cl, Br, and I). Among these predicted materials, tens of ferromagnetic semiconducting monolayers were proposed including MAT_3-type $CrSnTe_3$ (170 K)[17] and $CrGeS_3$ (161 K),[19] MX_3-type $CrBr_3$ (73 K) and $CrCl_3$ (49 K),[20] and MX_2-type $NiCl_2$ (138 K), $NiBr_2$ (132 K), $CoCl_2$ (85 K), and $CoBr_2$ (23 K).[21] Nevertheless, they all take a T_c lower than 200 K. On the other hand, the 4d or 5d transition metal based MAT_3-type $TcSiTe_3$[28] and MX_3-type $PdBr_3$ and $PtBr_3$[29] have been predicted as ferromagnetic semiconductors with Curie temperatures above room temperature being 538 K, 350 K, and 375 K, respectively. They all take small bandgaps being less than 0.4 eV. Moreover, 1T-type MT_2 monolayers (like $CrSe_2$, $CrTe_2$, VS_2, and VSe_2[23–27]) have a higher T_c but show a metallic behavior. Experimentally, monolayer VSe_2 has been grown on highly oriented pyrolytic graphite or MoS_2 successfully, which takes 1T structure and is a ferromagnetic metal above 300 K.[26] A very recent study reported a group of 1T-type structures with mixed ligands, *i.e.*, 1T-MXY prototype.[30] The predicted Curie temperatures of these variant 1T structures can reach the room temperature. Unfortunately, all those proposed 2DFMSs with temperatures above 200 K or even room temperature have not yet been synthesized experimentally. Therefore, more candidate materials need to be proposed or new idea for designing two-dimensional ferromagnetic semiconductor candidates need to be attempted theoretically.

In this work, we proposed a new two-dimensional (2D) ferromagnetic semiconductor Li_2NiSe_2, which can be denoted as Li-decorated 1T-type $NiSe_2$ monolayer. We studied systematically the structure, magnetic, and electronic properties of the Li_2NiSe_2 monolayer by using first-principles electronic structure calculations. The results show that the Li_2NiSe_2 monolayer has a dynamically stable structure, intrinsic fer-

[†]Corresponding author. E-mail: hcyang@ruc.edu.cn
[‡]Corresponding author. E-mail: zlu@ruc.edu.cn

© 2023 Chinese Physical Society and IOP Publishing Ltd

romagnetic ground state, and indirect band gap of medium size. The thermal dependence of magnetic properties and the Curie temperature of magnetic transition are estimated by using the statistical Monte Carlo (MC) simulations based on the classical Heisenberg model and the T_c is up to 307 K. The origin of the ferromagnetism is discussed with the theory of magnetic exchange based on the Goodenough–Kanamori–Anderson (GKA) rules.[31–36]

2. Computational methods

The first-principles electronic structure calculations were performed in the framework of density functional theory (DFT) using the Vienna *ab-initio* simulation package (VASP).[37,38] The generalized gradient approximation (GGA) of Perdew–Burke–Ernzerhof (PBE) type was adopted for the exchange–correlation functional.[39] The projector augmented wave (PAW) method[40,41] was adopted to describe the interactions between valence electrons and nuclei. The kinetic energy cutoff of the plane-wave basis was set to be 650 eV. The total energy convergence and the atomic force tolerance were set to be 10^{-6} eV and 0.01 eV/Å, respectively. For describing the Fermi–Dirac distribution function, a Gaussian smearing of 0.02 eV was used. The $13 \times 13 \times 1$ gamma-centered Monkhorst–Pack grids[42] were used for the Brillouin zone (BZ) sampling of the primitive cell. We adopted a vacuum distance about 40 Å in the c direction to eliminate the interactions between adjacent layers in the slab modeling the 2D systems. To check the correlation effects of Ni-3d orbitals, we also performed GGA+U calculations by using the simplified rotationally invariant version of Dudarev *et al.*[43] The phonon spectra was additionally simulated by PHONOPY[44] and the force constants were calculated based on the density functional perturbation theory with a $4 \times 4 \times 1$ supercell. To investigate the thermal stability of the Li_2NiSe_2, *ab-initio* molecular dynamics (AIMD) simulations were carried out at 300 K using canonical ensemble (NVT). The total simulation time is 5 ps with a timestep of 1 fs. The spin–orbital coupling (SOC) was considered in the magnetocrystalline anisotropy energy (MAE) and exchange interaction calculations. The Monte Carlo simulations based on the classical Heisenberg model were employed to describe the thermal dynamics of magnetism in equilibrium state[45,46] for which the open source project MCSOLVER code was used.[47]

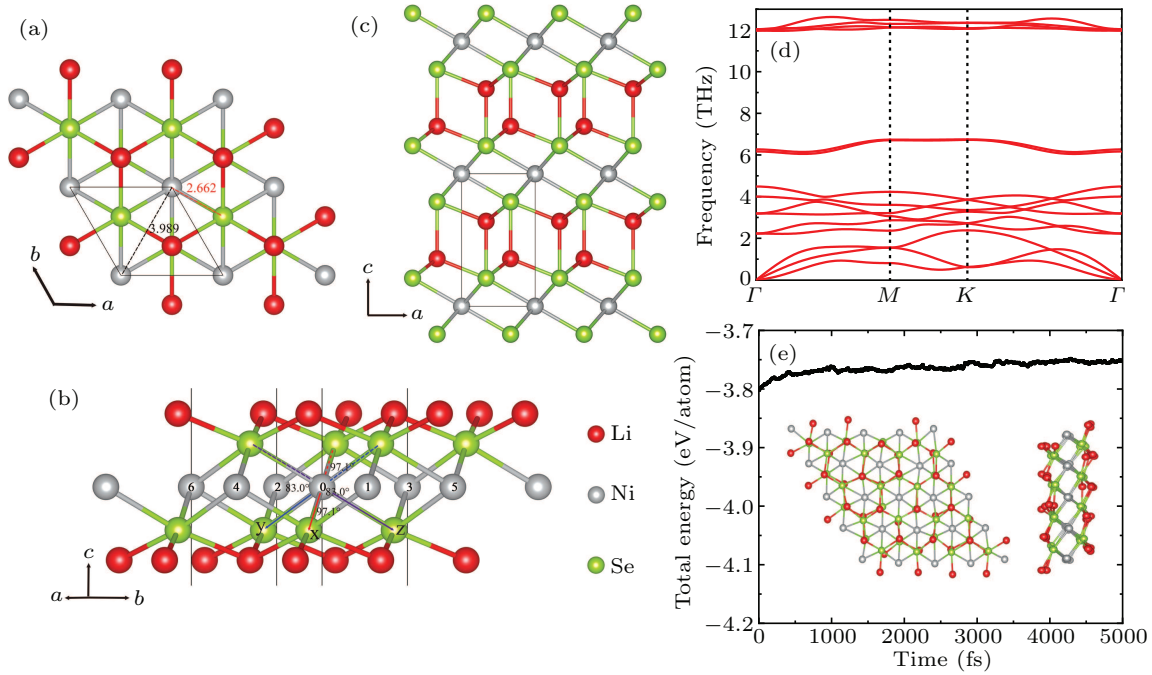


Fig. 1. Crystal structure of Li_2NiSe_2: (a) top view of monolayer, (b) side view of monolayer, and (c) side view of bulk, (d) phonon dispersions of monolayer Li_2NiSe_2, (e) the fluctuation of total energy of monolayer Li_2NiSe_2 and the snapshot for the final configuration after AIMD simulation at 300 K. The coordinate indices and atomic numbers in panel (b) correspond to those in Fig. 6(b).

3. Results and analyses

3.1. Crystal structure and stability

The prototype compound Li_2NiO_2[48,49] has been synthesized experimentally and it takes an intra-layer ferromagnetic but interlayer antiferromagnetic order.[49] The Li_2NiSe_2 is derived from Li_2NiO_2 by replacing O by Se. As a result, the bulk Li_2NiSe_2 takes a triangular lattice (Fig. 1(c), space group #164, P-3m1) with a fivefold layered structure in the c direction. Each Ni atom is located in an octahedral field formed by six Se atoms while each Li atom is in the off-center position of a stretched tetrahedral field. After full relaxation, the lattice parameters of Li_2NiSe_2 are $a = 3.980$ Å and $c = 6.201$ Å, respectively, which are larger than those of Li_2NiO_2 ($a = 3.134$ Å, and $c = 5.010$ Å). The calcu-

lated formation enthalpy of Li_2NiSe_2, which is defined as $\Delta E_f = E_{Li_2NiSe_2} - 2E_{Li} - E_{Ni} - 2E_{Se}$, where E_{Li}, E_{Ni}, and E_{Se} are respectively the energies of elements Li, Ni, and Se, $E_{Li_2NiSe_2}$ is the energy of the bulk Li_2NiSe_2 per chemical formula, is −3.23 eV/f.u. The negative formation enthalpy indicates that this is an exothermic reaction and Li_2NiSe_2 is less reactive. When Li_2NiSe_2 is reduced to an atomic-layer thin film, with an Li–Se–Ni–Se–Li fivefold layered structure as shown in Figs. 1(a) and 1(b), the relaxed lattice constant is 3.989 Å using a supercell with 40-Å vacuum distance in the c direction. Structurally, the monolayer Li_2NiSe_2 can be denoted as Li-decorated 1T-type monolayer $NiSe_2$. To be specific, the Ni–Se bond length is 2.662 Å while the distance between two nearest Ni atoms is 3.989 Å. This suggests that there is a weak direct exchange but a strong superexchange between two nearest Ni atoms. The bond angles for both Ni–Se–Ni and Se–Ni–Se are around 90° (see Fig. 1(b)), suggesting that the superexchange coupling may be ferromagnetic based on the GKA rules.[31–36] To estimate its exfoliation feasibility, we calculated the cleavage energy by using DFT-D2[50] to mimic the long range van der Waals interactions, which is about 0.81 J/m^2 and comparable to those of layered materials like h-BN (0.45 J/m^2), $NbSe_2$ (0.40 J/m^2), and graphite (0.37 J/m^2), suggesting the possibility of cleaving into monolayer. Lattice dynamics was studied by using PHONOPY and the phonon dispersion is shown in Fig. 1(d). The negligible imaginary frequencies around the Γ point, since the supercell used to simulate lattice dynamics has a limited size, demonstrate the dynamical stability of the monolayer Li_2NiSe_2. Figure 1(e) displays top and side view snapshots of the structure, as well as the evolution of the total energy over the 5-ps simulation time. There is no structural destruction, which indicates that the Li_2NiSe_2 monolayer has a good thermal stability at 300 K.

3.2. Magnetic properties

To study the magnetic properties of the Li_2NiSe_2 monolayer, we carried out spin-polarized calculations on five magnetic configurations, one FM state and four AFM states as shown in Fig. 2, to identify its ground state. The unit cell of each AFM configuration is shown in the black box in Fig. 2. Among these five magnetic configurations, the calculations show that the FM state takes the lowest energy, thus being the ground state. The energy differences of the four AFM states with respect to the FM state ($\Delta E = E_{AFM} - E_{FM}$) are shown in Fig. 3.

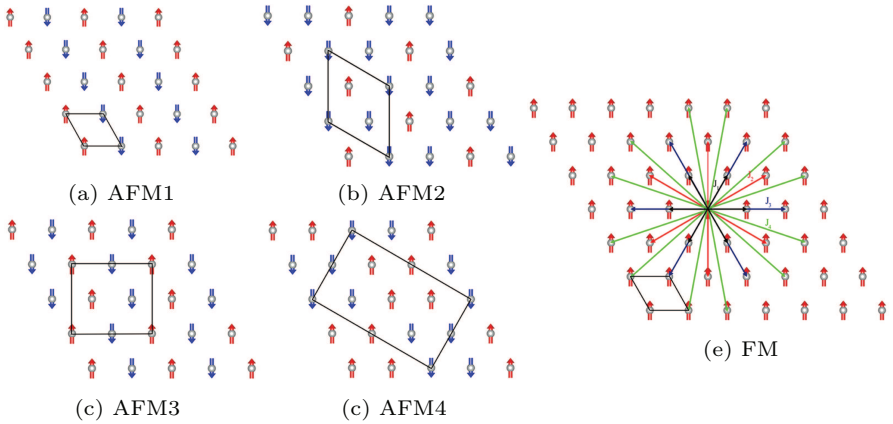


Fig. 2. Top view of four AFM magnetic configurations and FM configuration. Only Ni atoms are shown for simplicity. The unit cell of these magnetic configurations are outlined by blank lines. the first-, second-, third-, and fourth-nearest neighbors are marked by black, red, blue, and green solid lines in panel (e).

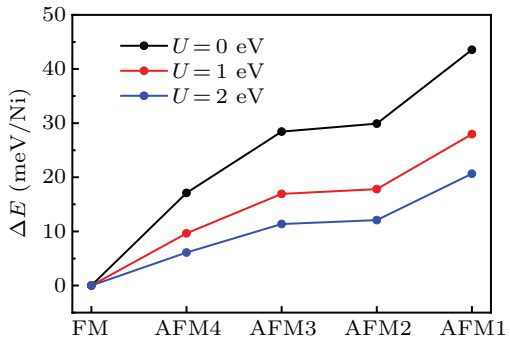


Fig. 3. The energy differences of the AFM states with respect to the FM state, *i.e.*, $\Delta E = E_{AFM} - E_{FM}$.

The AFM1 state takes the highest energy, being about 42 meV/Ni larger than that of the FM state. The calculated magnetic moments are about 1.22 μ_B and 0.22 μ_B on each Ni and Se atoms, respectively, while the magnetic moments on the Li atoms are negligible. The magnetic moments on the Se atoms are mainly from the polarization of their p orbitals due to the p–d hybridization between the Se and Ni atoms as shown in Fig. 5(a). The magnetocrystalline anisotropy energy (MAE) was calculated to be 0.23 meV/f.u., which is in the same order of magnitude as the ones of the Fe (0.10±0.05 meV) and Co (0.15±0.02 meV) monolayers on the Pt (111) substrates.[51] The easy magnetization direction is lying in the plane.

One of the important properties of ferromagnets is the Curie temperature T_c. We adopted a classical anisotropic Heisenberg model to estimate the T_c of Li_2NiSe_2. The Hamil-

tonian is shown as follows:

$$H = \sum_{\langle i,j\rangle,\alpha} J_1^\alpha S_i^\alpha S_j^\alpha + \sum_{\langle\langle i,j\rangle\rangle,\alpha} J_2^\alpha S_i^\alpha S_j^\alpha + \sum_{\langle\langle\langle i,j\rangle\rangle\rangle,\alpha} J_3^\alpha S_i^\alpha S_j^\alpha + \sum_{\langle\langle\langle\langle i,j\rangle\rangle\rangle\rangle,\alpha} J_4^\alpha S_i^\alpha S_j^\alpha + A^\alpha \sum_i \left(S_i^2\right),$$

where S_i represents the spin of Ni ion on the i-th site, α labels directions x, y, and z, A^α is the easy-axis single ion anisotropy factor, and J_1, J_2, J_3, and J_4 denote the first-, second-, third-, and fourth-nearest exchange interaction parameters, respectively. All J_i^α and A^α values were derived from the mapping analysis of five different magnetic configurations with considering the SOC (FM, AFM1-4, Fig. 2) to the above Heisenberg model. The total energies per Ni atom for the five mentioned magnetic configurations can be written using the following equations:

$$\begin{aligned}
E_{\mathrm{FM}}^\alpha &= (3J_1^\alpha + 3J_2^\alpha + 3J_3^\alpha + 6J_4^\alpha + A^\alpha)\,|S|^2 + E_0,\\
E_{\mathrm{AFM1}}^\alpha &= (-J_1^\alpha - J_2^\alpha + 3J_3^\alpha - 2J_4^\alpha + A^\alpha)\,|S|^2 + E_0,\\
E_{\mathrm{AFM2}}^\alpha &= (-J_1^\alpha + 3J_2^\alpha - J_3^\alpha - 2J_4^\alpha + A^\alpha)\,|S|^2 + E_0,\\
E_{\mathrm{AFM3}}^\alpha &= (-J_1^\alpha + J_2^\alpha - J_3^\alpha + 2J_4^\alpha + A^\alpha)\,|S|^2 + E_0,\\
E_{\mathrm{AFM4}}^\alpha &= (-J_3^\alpha + A^\alpha)\,|S|^2 + E_0,
\end{aligned}$$

where E_0 is the energy excluding the magnetic coupling that is not sensitive to different magnetic configurations. This is solved to give

$$\begin{aligned}
J_1^\alpha\,|S|^2 &= \frac{1}{8}E_{\mathrm{FM}}^\alpha - \frac{1}{8}E_{\mathrm{AFM1}}^\alpha - \frac{1}{2}E_{\mathrm{AFM3}}^\alpha + \frac{1}{2}E_{\mathrm{AFM4}}^\alpha,\\
J_2^\alpha\,|S|^2 &= \frac{1}{16}E_{\mathrm{FM}}^\alpha - \frac{1}{16}E_{\mathrm{AFM1}}^\alpha + \frac{1}{4}E_{\mathrm{AFM2}}^\alpha - \frac{1}{4}E_{\mathrm{AFM4}}^\alpha,\\
J_3^\alpha\,|S|^2 &= \frac{1}{16}E_{\mathrm{FM}}^\alpha + \frac{3}{16}E_{\mathrm{AFM1}}^\alpha - \frac{1}{4}E_{\mathrm{AFM4}}^\alpha,\\
J_4^\alpha\,|S|^2 &= \frac{1}{32}E_{\mathrm{FM}}^\alpha - \frac{1}{32}E_{\mathrm{AFM1}}^\alpha - \frac{1}{8}E_{\mathrm{AFM2}}^\alpha + \frac{1}{4}E_{\mathrm{AFM3}}^\alpha - \frac{1}{8}E_{\mathrm{AFM4}}^\alpha,\\
E_0 + A^\alpha\,|S|^2 &= \frac{1}{16}E_{\mathrm{FM}}^\alpha + \frac{3}{16}E_{\mathrm{AFM1}}^\alpha + \frac{3}{4}E_{\mathrm{AFM4}}^\alpha.
\end{aligned}$$

We take A^x as the reference value of single ion anisotropy energy, *i.e.*, set $A^x = 0$. Then,

$$A^{y,z} = \frac{1}{16}\left(E_{\mathrm{FM}}^{y,z} - E_{\mathrm{FM}}^x\right) + \frac{3}{16}\left(E_{\mathrm{AFM1}}^{y,z} - E_{\mathrm{AFM1}}^x\right) + \frac{3}{4}\left(E_{\mathrm{AFM4}}^{y,z} - E_{\mathrm{AFM4}}^x\right)$$

can be used to describe the strength of single ion anisotropy energy.

The exchange interaction parameters and single ion anisotropy factors are listed in Table 1, in which the magnitudes of S_i and S_j are set to 1. By using Metropolis Monte Carlo (MC) simulations based on the above 2D Heisenberg model, we calculated the Curie temperature of Li_2NiSe_2 monolayer by using a 100×100 supercell. Figure 4 shows the evolution of the normalized S and auto-correlation along with temperature. The Curie temperature can be extracted from the peak of the auto-correlation, *i.e.*, 307 K. The T_c of Li_2NiSe_2 is obviously higher than that of 1T-type MX_2 monolayers $NiCl_2$, $NiBr_2$, and NiI_2 (138 K, 132 K, 129 K[21]). To benchmark the calculation of Curie temperature for Li_2NiSe_2, we have also calculated the T_c of $NiBr_2$ by using the above method and the calculated T_c is 123 K, which is close to the value 132 K from Ref. [21].

Table 1. Anisotropic exchange constants up to the fourth nearest neighbor and single ion anisotropy factors in unit meV, in which the magnitudes of S_i and S_j are set to 1.

	1NN	2NN	3NN	4NN
J_x (meV)	–15.97	–2.86	1.86	–1.67
J_y (meV)	–15.91	–2.85	1.84	–1.69
J_z (meV)	–15.94	–2.85	1.86	–1.68
A^y (meV)	–0.025			
A^z (meV)	0.163			

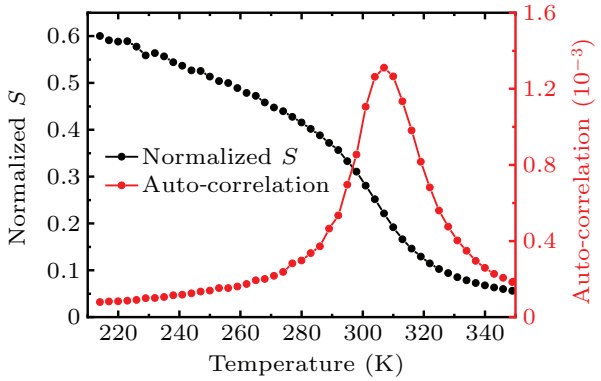


Fig. 4. The evolution of the normalized S and auto-correlation along with temperatures.

3.3. Electronic properties

We further study the electronic properties of the monolayer Li_2NiSe_2. The vanishing density of states at the Fermi level indicates that Li_2NiSe_2 is an intrinsic semiconductor with a bandgap of 0.51 eV as shown in Fig. 5(a). Near the valence band maximum (VBM) and conduction band minimum (CBM), both the Ni-3d orbitals and the Se-4p orbitals contribute to the density of states, but the Ni-3d orbitals dominate the CBM, while the contribution of Li atoms to the density of states is negligible. The overlap of the Ni-3d and Se-4p orbitals in a large energy range demonstrates the significant 3d–4p hybridization between them. On the other hand, the differential charge density in Fig. 5(d) shows that the electron depletes around the Ni atoms and accumulates in the region of Ni–Se bonds and Li–Se bonds. This also confirms the 3d–4p hybridization between the Ni and Se atoms and indicates the Li–Se covalent bonding feature. We notice that the valence bands and conduction bands near the band edge have different spin polarizations, as shown in Fig. 5(c), which enables creating and controlling completely spin-polarized currents with reversible spins simply by applying a gate voltage, suggesting that the monolayer Li_2NiSe_2 can act as a bipolar magnetic semiconductor.[52,53]

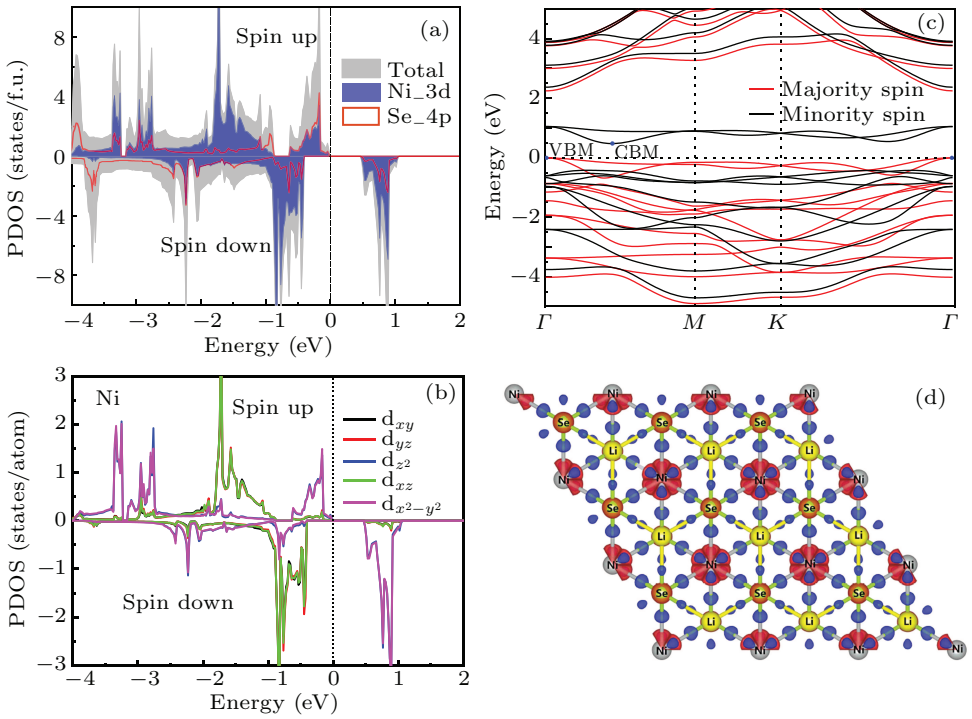


Fig. 5. (a) Density of states of the Ni-3d and Se-4p orbitals, (b) projected density of states (PDOS) of the Ni-3d orbitals, and (c) spin-resolved band structure of the FM Li_2NiSe_2 monolayer. (d) Top view of the differential charge density of the FM Li_2NiSe_2 monolayer, where the blue and red regions respectively denote the electron accumulation and depletion with the isosurface being set to 0.008 e/Å^3.

4. Discussion

The ferromagnetism of the Li_2NiSe_2 monolayer can be understood from its electronic structure. In the Li_2NiSe_2 monolayer, each Ni atom is surrounded by six Se neighbors which form a nearly spherical octahedral coordination, and then the Ni-3d orbitals are splited into two parts, namely the lower 3-fold t_{2g} (d_{xy}, d_{yz}, and d_{xz}) and the higher 2-fold e_g (d_{z^2} and $d_{x^2-y^2}$), according to the crystal field theory.[54–57] The strong p–d hybridization shifts the spin-majority e_g states well down, resulting in an energy sequence of Ni-3d orbitals roughly as spin-majority e_g states, spin majority t_{2g} states, spin-minority t_{2g} states, and spin-minority e_g states, as shown in Figs. 5(b) and 6(a). Nominally, in Li_2NiSe_2, each Ni atom has 8 d electrons and thus both the majority and minority spin channels of the t_{2g} states are occupied, while only the majority spin channel of the e_g states is occupied, resulting in a 2-μ_B magnetic moments on each Ni atom according to the Hund's rule.[33] There are two distinct mechanisms that determine the magnetic properties of the Li_2NiSe_2 monolayer as follows: (i) the direct exchange between two nearest Ni atoms and (ii) the selenium-mediated Ni–Se–Ni superexchange interactions. Due to the large distance between the two nearest Ni atoms (Ni–Ni bond 3.98 Å), the direct exchange is very weak. Thus, the Ni–Se–Ni superexchange dominates the magnetic properties of Li_2NiSe_2. Based on the Goodenough–Kanamori–Anderson (GKA) rules,[31–36] the superexchange mechanism in Li_2NiSe_2 can be further elaborated by following the process, as shown in Figs. 6(b)–6(d). There are three kinds of superexchange scenarios based on different involved orbitals between the two nearest Ni atoms. The first mechanism (SE1, Fig. 6(c)) can be expressed as (e_g–p_x)/(p_y–e_g), which means that the e_g states of the two Ni atoms will form σ bonds with on-site p_x and p_y states in the same ligand. Such a σ bond allows the spin-down electrons to hop into the unoccupied e_g states from the p orbitals. Meanwhile, the spin-up electrons remaining in the p_x/p_y states exchange with each other ferromagnetically based on the Hund's rule for such on-site orthogonal orbitals, resulting in a ferromagnetic coupling between the Ni atoms. The second and third superexchange processes (SE2 and SE3, Fig. 6(d)) can be presented as [e_g–p_y(p_x)]/(p_z–e_g), where the electron hopping still happens between (e_g–p_x)/p_y]/p_z via covalent σ bond, and the ferromagnetic order is also maintained by the on-site p_y(p_x) and p_z exchange. All three superexchange processes, with near 90° anion-mediated Ni–Se–Ni bond angles, result in relatively strong FM coupling (comparing to π bonds). Due to the dominating FM superexchange, the system takes FM.

To examine the correlation effects of Ni-3d electrons, we further did GGA+U calculations with U = 1 eV and 2 eV. For both U values, the FM state is still the ground state, as shown in Fig. 3. The energy differences between the FM and those AFM states decrease with the increase of U value. This is because of the weakening of ferromagnetic superexchange interactions. Then, the resulting estimated T_c values are 288 K and 241 K for U being 1 eV and 2 eV, respectively, which are lower than that without U. On the other hand, the calculated density of states and electronic band dispersions are overall similar for

$U = 0$ eV, 1 eV, and 2 eV except for the small and predictable change in the band gap and exchange splitting. Since the density of states of the occupied Ni-3d orbitals is broadened in a large energy range, moreover they have significant 3d–4p hybridization between the Ni and Se atoms, we infer that the correlation effect of Ni-3d orbitals in Li_2NiSe_2 is unimportant and the results calculated with small U values even without U are more reasonable.

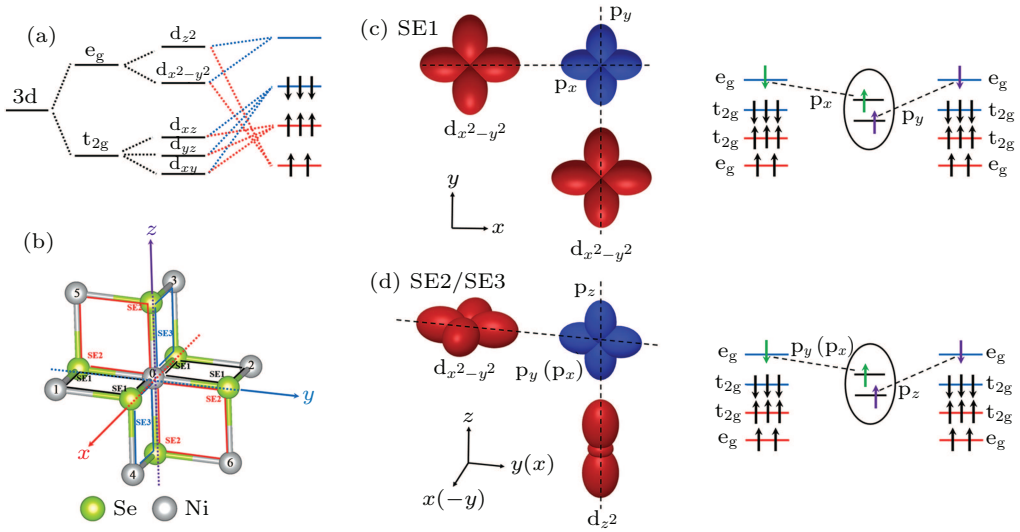


Fig. 6. Schematic representations of (a) Ni-3d orbitals splitting and (b)–(d) Ni–Se–Ni superexchange (SE) processes.

We also studied the electronic and magnetic properties of the monolayer Li_2NiO_2 and Li_2NiS_2, which are the analogs of the monolayer Li_2NiSe_2 based on the same prototype. The calculated cleavage energies for the monolayer Li_2NiO_2 and Li_2NiS_2 are 1.88 J/m^2 and 1.03 J/m^2, respectively, which are both larger than that of Li_2NiSe_2 (0.81 J/m^2), suggesting that Li_2NiSe_2 is more feasible to be cleaved into monolayer. The phonon spectrum calculations show that both the monolayer Li_2NiO_2 and Li_2NiS_2 are dynamically stable. Considering that the prototype compound Li_2NiO_2[48,49] has been synthesized experimentally, together with the moderate cleavage energies and the dynamical stability of the monolayers Li_2NiO_2, Li_2NiS_2, and Li_2NiSe_2, we speculate that the experimental preparation of the monolayers Li_2NiO_2, Li_2NiS_2, especially Li_2NiSe_2 is promising. For both the monolayers Li_2NiO_2 and Li_2NiS_2, the FM state takes the lowest energy among the five magnetic structures that we studied and should be the ground state. The band structure calculations show that they are both indirect band gap semiconductors with the band gaps being 1.16 eV and 0.64 eV, respectively in their ground states. The calculated Curie temperatures for the monolayers Li_2NiO_2 and Li_2NiS_2 are 22 K and 134 K, respectively, which are lower than that of Li_2NiSe_2 (307 K). This is because the p orbitals of O and S are not as extended as those of Se, resulting in the weakening of p–d hybridization and thus the weakening of the Ni–chalcogen–Ni FM superexchange.

5. Conclusion

In summary, we have investigated the structural, electronic, and magnetic properties of monolayer Li_2NiSe_2 using first-principles electronic structure calculations. We find that the monolayer Li_2NiSe_2 is an intrinsic ferromagnetic semiconductor. The structure of monolayer Li_2NiSe_2 is derived from the synthesized prototype compound Li_2NiO_2 by replacing O with Se, and it is dynamically stable. Its magnetic properties are dominated by the Ni–Se–Ni FM superexchange. The Curie temperature is estimated to be above 200 K by the Monte Carlo simulations based on the Heisenberg model. Structurally, the monolayer Li_2NiSe_2 can be denoted as Li-decorated monolayer 1T-type $NiSe_2$, suggesting a new choice to design two-dimensional ferromagnetic semiconductors.

Acknowledgements

Project supported by the National Key Research and Development Program of China (Grant No. 2019YFA0308603), and the National Natural Science Foundation of China (Grant No. 11934020). Computational resources were provided by the Physical Laboratory of High Performance Computing at Renmin University of China.

References

[1] Li X and Yang J 2017 *WIREs Comput. Mol. Sci.* **7** 1
[2] Fert A 2008 *Rev. Mod. Phys.* **80** 1517
[3] Feng Y P, Shen L, Yang M, Wang A, Zeng M, Wu Q, Chintalapati S and Chang C R 2017 *WIREs Comput. Mol.* **7** 1
[4] Zhao Y, Zhang J J, Yuan S and Chen Z 2019 *Adv. Funct. Mater.* **29** 1901420
[5] Gong C and Zhang X 2019 *Science* **363** 706
[6] Li H, Ruan S and Zeng Y 2019 *Adv. Mater.* **31** 1900065
[7] Zhao Y, Gu J and Chen Z 2019 *Adv. Funct. Mater.* **29** 1904782
[8] Zhang S, Xu R, Duan W and Zou X 2019 *Adv. Funct. Mater.* **29** 1808380

[9] Bader S D and Parkin S S 2010 *Annu. Rev. Condens. Matter Phys.* **1** 71
[10] Wolf S A, Awschalom D D, Buhrman R A, Daughton J M, Molnr S V, Roukes M L, Chtchelkanova A Y and Treger D M 2001 *Science* **294** 1488
[11] Huang B, Clark G, Navarro-Moratalla E, Klein D R, Cheng R, Seyler K L, Zhong D, Schmidgall E, McGuire M A, Cobden D H, Yao W, Xiao D, Jarillo-Herrero P and Xu X 2017 *Nature* **546** 270
[12] Zhang Z, Shang J, Jiang C, Rasmita A, Gao W and Yu T 2019 *Nano Lett.* **19** 3138
[13] Cai X, Song T, Wilson N P, Clark G, He M, Zhang X, Taniguchi T, Watanabe K, Yao W, Xiao D, McGuire M A, Cobden D H and Xu X 2019 *Rev. Mod. Phys.* **19** 3993
[14] Gong C, Li L, Li Z, Ji H, Stern A, Xia Y, Cao T, Bao W, Wang C, Wang Y, Qiu Z Q, Cava R J, Louie S G, Xia J and Zhang X 2017 *Nature* **546** 265
[15] Li X and Yang J 2014 *J. Mater. Chem. C* **2** 7071
[16] Sivadas N, Daniels M W, Swendsen R H, Okamoto S and Xiao D 2015 *Phys. Rev. B* **91** 235425
[17] Zhuang H L, Xie Y, Kent P R C and Ganesh P 2015 *Phys. Rev. B* **92** 035407
[18] Chittari B L, Lee D, Banerjee N, MacDonald A H, Hwang E and Jung J 2020 *Phys. Rev. B* **101** 085415
[19] Ren Y, Ge Y, Wan W, Li Q and Liu Y 2019 *J. Phys.: Condens. Matter* **32** 015701
[20] Zhang W B, Qu Q, Zhu P and Lam C H 2015 *J. Mater. Chem. C* **3** 12457
[21] Kulish V V and Huang W 2017 *J. Mater. Chem. C* **5** 8734
[22] Botana A S and Norman M R 2019 *Phys. Rev. Mater.* **3** 044001
[23] Ma Y, Dai Y, Guo M, Niu C, Zhu Y and Huang B 2012 *ACS Nano* **6** 1695
[24] Zhang H, Liu L M and Lau W M 2013 *J. Mater. Chem. A* **1** 10821
[25] Zhuang H L and Hennig R G 2016 *Phys. Rev. B* **93** 054429
[26] Bonilla M, Kolekar S, Ma Y, Diaz H C, Kalappattil V, Das R, Eggers T, Gutierrez H R, Phan M H and Batzill M 2018 *Nat. Nanotechnol.* **13** 289
[27] Lv H Y, Lu W J, Shao D F, Liu Y and Sun Y P 2015 *Phys. Rev. B* **92** 214419
[28] You J Y, Zhang Z, Dong X J, Gu B and Su G 2020 *Phys. Rev. Res.* **2** 013002
[29] You J Y, Zhang Z, Gu B and Su G 2019 *Phys. Rev. Appl.* **12** 024603
[30] Xiao J, Legut D, Luo W, Guo H, Liu X, Zhang R and Zhang Q 2020 *Phys. Rev. B* **101** 014431
[31] Rado G T and Suhl H 1963 *Magnetism* (New York: Harcourt Brace Jovanovich) pp. 67–68
[32] Goodenough J 1963 *Magnetism and the chemical bond* (Chichester: John Wiley and Sons) pp. 168–184
[33] Coey J M, Venkatesan M and Fitzgerald C B 2005 *Nat. Mater.* **4** 173
[34] Deng H X, Li J, Li S S, Xia J B, Walsh A and Wei S H 2010 *Appl. Phys. Lett.* **96** 162508
[35] Walsh A, Silva J L F D and Wei S H 2008 *Phys. Rev. Lett.* **100** 256401
[36] Albaridy R, Manchon A and Schwingenschlögl U 2020 *J. Phys.: Condens. Matter* **32** 355702
[37] Kresse G and Furthmüller J 1996 *Comput. Mater. Sci.* **6** 15
[38] Kresse G and Furthmüller J 1996 *Phys. Rev. B* **54** 11169
[39] Perdew J P, Burke K and Ernzerhof M 1996 *Phys. Rev. Lett.* **77** 3865
[40] Blöchl P E 1994 *Phys. Rev. B* **50** 17953
[41] Kresse G and Joubert D 1999 *Phys. Rev. B* **59** 1758
[42] Monkhorst H J and Pack J D 1976 *Phys. Rev. B* **13** 5188
[43] Anisimov V I, Aryasetiawan F and Lichtenstein A I 1997 *J. Phys.: Condens. Matter* **9** 767
[44] Togo A and Tanaka I 2015 *Scr. Mater.* **108** 1
[45] Kan M, Adhikari S and Sun Q 2014 *Phys. Chem. Chem. Phys.* **16** 4990
[46] Kan M, Zhou J, Sun Q, Kawazoe Y and Jena P 2013 *J. Phys. Chem. Lett.* **4** 3382
[47] Liu L, Ren X, Xie J, Cheng B, Liu W, An T, Qin H and Hu J 1991 *Appl. Surf. Sci.* **480** 300
[48] Davidson I, Greedan J E, von Sacken U, Michal C A and Dahn J R 1991 *Solid State Ionics* **46** 243
[49] Davidson I J, Greedan J E, Sacken U V, Michal C A and McKinnon W R 1993 *J. Solid State Chem.* **105** 410
[50] Grimme S 2006 *J. Computat. Chem.* **27** 1787
[51] Lehnert A, Dennler S, Błoński P B, Rusponi S, Etzkorn M, Moulas G, Bencok P, Gambardella P, Brune H and Hafner J 2010 *Phys. Rev. B* **82** 094409
[52] Li X and Yang J 2013 *Phys. Chem. Chem. Phys.* **15** 15793
[53] Li X, Li X and Yang J 2020 *J. Phys. Chem. Lett.* **11** 4193
[54] Hu X, Zhao Y, Shen X, Krasheninnikov A V, Chen Z and Sun L 2020 *ACS Appl. Mater. Interfaces* **12** 26367
[55] Zhang X, Wang B, Guo Y, Zhang Y, Chen Y and Wang J 2019 *Nanoscale Horiz.* **4** 859
[56] Xu X, Ma Y, Zhang T, Lei C, Huang B and Dai Y 2020 *Nanoscale Horiz.* **5** 1386
[57] Liu N, Zhou S and Zhao J 2020 *Phys. Rev. Mater.* **4** 094003